APPLICATION OF SURFACE STRAIN GAGES AT THE FAA'S NAPTF

By:
Edward Guo
SRA International, 3120 Fire Road
Egg Harbor Township, 08234, NJ, U.S.A.
Phone: (609) 645-3772 -120
Fax: (609) 645-2881
Edward_guo@SRA.com

and

Frank Pecht
Federal Aviation Administration,
Airport Technology R&D Branch, AJP-6310
William J. Hughes Technical Center,
Atlantic City, New Jersey, USA
Phone: (609) 485-8503
Fax: (609) 485-8555
Frank.pecht@faa.gov

PRESENTED FOR THE
2007 FAA WORLDWIDE AIRPORT TECHNOLOGY TRANSFER CONFERENCE
Atlantic City, New Jersey, USA

April 2007

ABSTRACT

Since 1999, over a thousand embedded concrete strain gages have been used at the FAA's NAPTF. However, two issues have to be considered. First, extrapolation of the data, rather than direct measurement, has to be used to obtain the critical strain at slab surface. Second, each gage costs more than 500 dollars necessitating a reduction in the amount of strain gages to satisfy budgetary requirements. To alleviate these concerns, surface strain gages have been used since 2004. The cost of each gage is typically less than ten dollars, and its reliability is similar to the embedded gages if they are used appropriately. Seven surface gages were installed at a transverse joint and one at a longitudinal joint of a 17" thick slab. Two-step static gear loads and slow rolling loads were used to get strain histories. Two, four and six wheels were used for both static and slow rolling tests. The test data verifies the findings at NAPTF in 2000: The gear load dominates both top-down and bottom-up cracks at transverse joints, and it only dominates the top-down cracks while the wheel load dominates the bottom-up cracks at longitudinal joints. Comparisons between the recorded strains under static and slow rolling load show that the magnitude of strain history under a slow rolling load matches the measured static strain very well if the load location is properly selected. The measured and calculated strains based on thin plate model at the longitudinal joint under a slow rolling load match well. However, the measured and calculated strains at the transverse joint only match well for the strain gage locations away from the load. They are poorly matched for the gage near the load. The discrepancy indicates that the thin plate model assumption might not be suitable in predicting surface strain near the load.

INTRODUCTION

Since 1999, over a thousand embedded concrete strain gages have been used at the FAA's National Airport Pavement Test Facility (NAPTF). However, two issues have to be considered. First, extrapolation of the data, rather than direct measurement, has to be used to obtain the critical strain at the slab surface. Recent research [3] indicates that surface stress may be high due to temperature as well as moisture variations. Therefore, directly measured surface strain becomes more desirable. Second, the cost of these full-bridge gages, more than 500 dollars, necessitates a reduction in the amount of strain gages to satisfy budgetary. To alleviate these concerns, inexpensive quarter bridge surface strain gages have been used since 2004. The cost of each gage is typically less than ten dollars, and its reliability over a short period of testing is similar to the embedded gages. Therefore, surface gages can be used for obtaining satisfactory critical responses at slab surface that can not be obtained by the embedded gages.

Three tests using surface strain gages have been conducted at the FAA's (NAPTF). The first one was performed in June 2004. The objective was to evaluate the reliability and durability of the surface gage and to gain experience in the proper installation of the gages. This was accomplished by comparing the strain histories recorded by embedded and surface gages under a slow rolling load.

Direct application of wheel loads on these surface gages requires considerable care in their installation. Grinding of the concrete surface accomplishes both the creation of a slight indentation as well as a smooth area for the application of the gage. The 120 mm gage is applied

on the prepared surface with the manufacturers recommended adhesive. At this point a coating of wax is placed on top of the gage which provides isolation between the gage and the protective epoxy covering that is then applied. In addition to the technique use on the gages, similar care is required to protect the gage leads from the wheel loading.

The second test was done in January 2005 in a North transition section. The slab size was 12.5 by 20 ft and thickness was 17 inches. Eight surface gages were installed to test the survivability of surface gages directly exposed to a slow rolling load. Strains under two, four and six wheels in different locations were recorded and compared for gear configuration analysis. Each strain history was continuously recorded from three round-trip loadings. In the first trip, two wheels were loaded and unloaded, and then four and six wheels were loaded and unloaded.

Two problems were encountered in analyzing the strain histories. First the amount of noise observed in all the surface strain records was higher than those in the embedded gages. This was probably caused by induced voltages associated with the proximity to the rather high power Vehicle distribution rails. Second, strain aberrations were observed between two loading trips. Consequently, the results were not completely satisfactory.

An additional, eight surface gages were applied on the South transition located more than sixty feet from the power rails in order to minimize the noise and aberration problem. Strains were again independently recorded for each loading pass.

In the third test, promising results were obtained. Seven surface gages were installed at a transverse joint and one at a longitudinal joint. Two-step static gear loads and slow rolling loads were used to obtain the strain histories. Single, two and four wheels were used for the static and two, four and six wheels for the slow rolling tests. The test data acquired using surface gages verified the findings that had been obtained at the NAPTF since 2000 using the embedded type of strain gage: In particular “the gear load dominates both top-down and bottom-up cracks at transverse joints, and it only dominates the top-down cracks while the wheel load dominates the bottom-up cracks at longitudinal joints.”

Comparisons between the recorded strains under static and slow rolling load show that the maximum value of strain history under a slow rolling load matches the measured static strain very well if the static load location is properly selected. The match of two types of results indicates that the dynamic effects under slow speed (5 miles/ hour, or 7.3 ft / second) on critical strain responses in concrete pavement can be neglected.

The measured and calculated strains using 2D finite element procedure [6] based on thin plate model for pavement surface layer [7] and dense liquid model for foundation [9] have also been compared to evaluate the suitability of the model. At the longitudinal joint under a slow rolling load they matched well. However, the measured and calculated strains at the transverse joint only match well for the strain gages located a distance away from the load. They are poorly matched for the gage near the load. The discrepancy indicates that the model assumptions may not be suitable in predicting surface strain near the load.

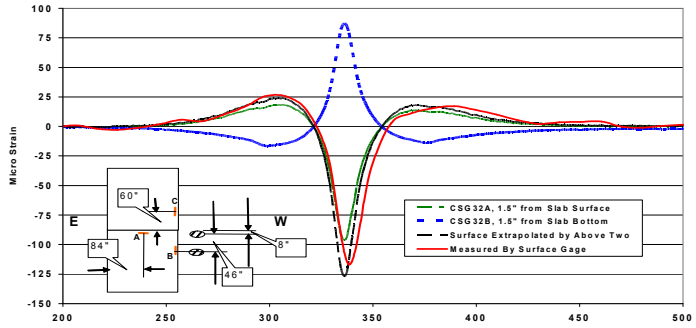

(a) Under a Two-Wheel Gear Load.

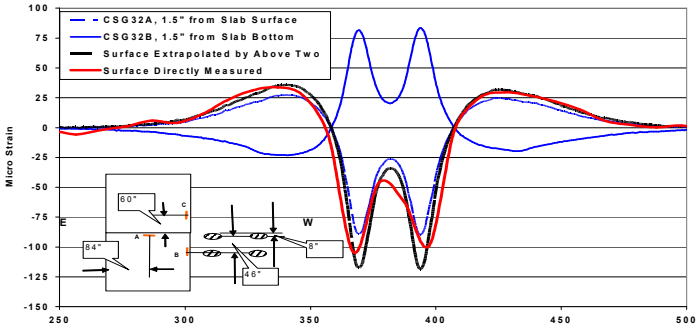

(b) Under a Four-Wheel Gear Load.

Figure 1. Comparisons of Strains Recorded by Embedded and Surface Strain Gages.

COMPARISON BETWEEN EMBEDDED AND SURFACE STRAIN GAGES

One surface gage was applied at A (Figure 1) above two embedded gages CSG32A (1.5" from slab surface) and CSG32B (1.5" from the slab bottom). Strain time histories were recorded simultaneously by the three gages. One wheel of the dual gear (two wheels) and two wheels of the two-dual gear (four wheels) were driven on above gages so critical strains were obtained. After assuming that the strains are linearly distributed along the slab depth, the strain at the slab surface can be extrapolated using equation (1):

$$\varepsilon_{SURFACE} = \varepsilon_B + (\varepsilon_A - \varepsilon_B) \times \frac{h - 1.5}{h - 2 \times 1.5} \quad (1)$$

Where ε_A, ε_B and $\varepsilon_{SURFACE}$ are strains measured by gages CSG32A, CSG32B and the surface gage at point A, and where h is the slab thickness which is equal to 12 inches.

Figure 1 shows that the surface strains extrapolated from ε_A and ε_B match the strains $\varepsilon_{SURFACE}$ well. The maximum compressive strain at the surface due to a two-wheel gear (125×10^{-6}) is larger than the strain due to a four-wheel gear (115×10^{-6}). We may extend the finding to the maximum strain at the bottom of the slab: the bottom strain under a two wheel gear is also larger than that under a four wheel gear. Second, the maximum tensile strain at the surface due to a

two-wheel gear is smaller than the maximum tensile strain due to a four-wheel gear. Many lower strain gages (similar to CSG32B) installed 1.5 inches from the slab bottom in test pavement CC1 (forty five 20 by 20 foot slabs, tested from 1999 to 2000) also show the same finding. The above finding is true because the contribution of the second axle to the maximum tensile strain at the slab bottom was negative; while the contribution to the maximum tensile strain at the slab surface was positive. The effects on the critical strains at transverse joints will be discussed later.

LESSONS LEARNED FROM THE TEST CONDUCTED IN JANUARY, 2005

Eight strain gages were used in the second test. Figure 2 shows the two north slabs of the test pavement, located in transition 5 which consisted of six slabs 12.5ft. By 20 ft, 17 inch thick. No cracks had been observed in the north and south two slabs. However, an end-to-end longitudinal crack was developed in the middle of the two middle slabs where heavy traffic loads had never been applied. The top-down crack was due to two heavy loads moving near the two longitudinal joints. Similar top-down cracks had been observed in February 2000 at the FAA NAPTF. Similar cracks have also been reported in [2] and [4]. More detailed information on the test pavement structure and testing results can be found in [5]. Wheel locations are given in Figure 3. Test 3 led to tensile strains in all surface gages at the transverse joint. Test 6 led to maximum bottom tensile strains at gage 3 and 6 since the two wheels drove on them. We shall discuss the results received from the above two tests.

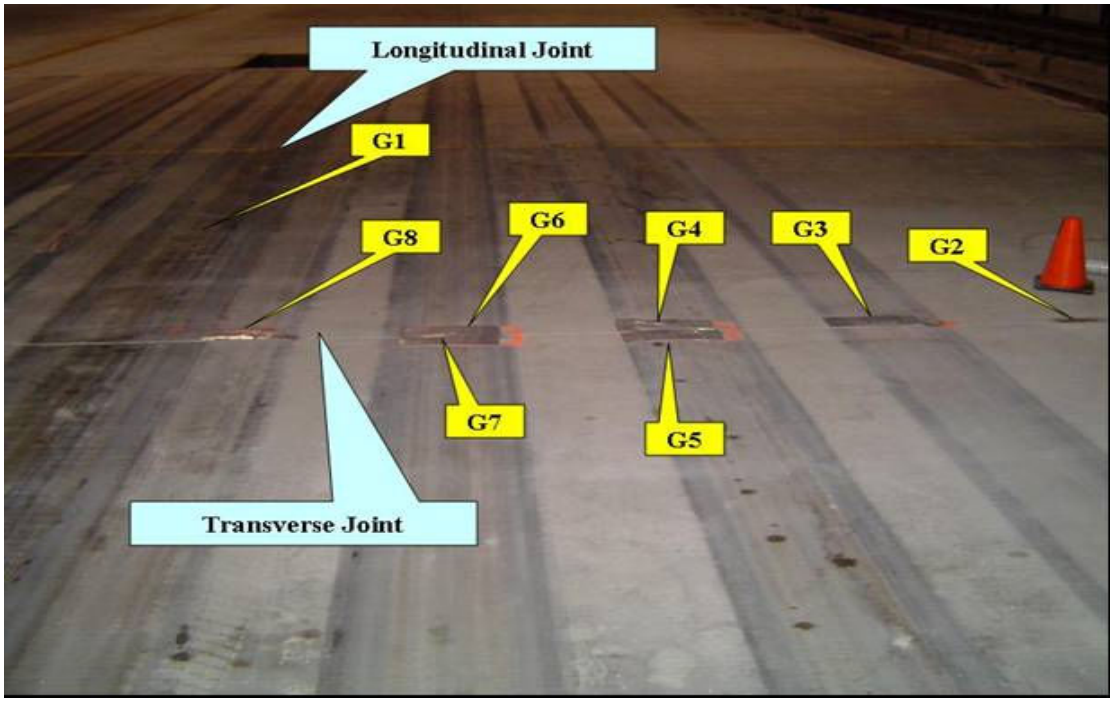

Figure 2. The Test Pavement – Transition 5.

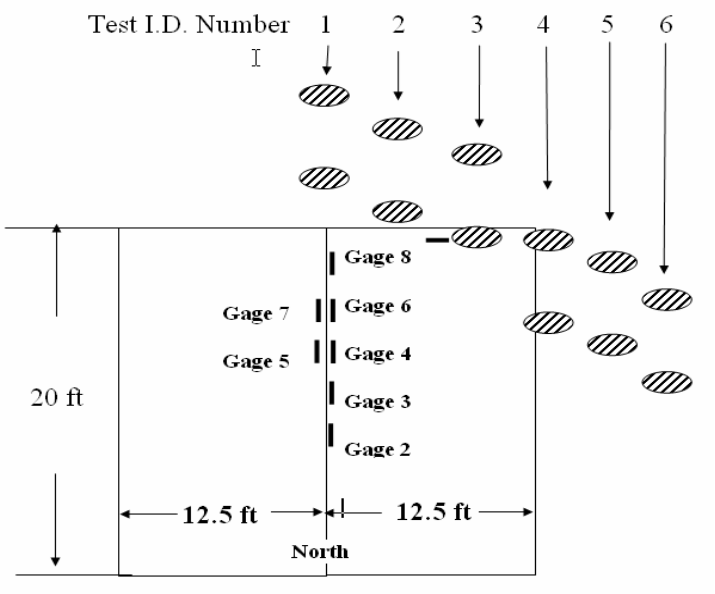

Figure 3. The Load and Strain Gage Locations.

Three tests were performed using 55,000 lb wheel loads. Each test with the vehicle consisted of three up and back passes beginning 25 feet west of the instrumented transverse joint. The first pass was with a dual wheel load (2 wheels) followed by a second pass with a two dual configuration (4 wheels) and finally with a three dual configuration (6 wheels). The speed of the test vehicle was 5 mph. The starting location of the vehicle loading was chosen in order to reduce the induced strain responses to a negligible magnitude. When the gear reached east far enough from the transverse joint, approximately 25 ft, the gear stopped but did not unload the pavement. Returning loaded to the west end of the test area the vehicle would unload then load with the next wheel configuration. After all three passes with the three different wheel configurations the data acquisition and test would end. Figure 4 (a) depicts the data acquired for test #3 Gage #6. A general comparison of the data acquired in test #3 and that obtained in Figure 1 shows a considerable increase in noise riding on the acquired data. In addition offset jumps can be observed in the data in Figure (4a), in particular when the gear was at the west starting location. Since these offsets did not occur at the east end, where the load remained constant, it has been concluded that these aberrations were the result of the vehicle loading and unloading. Consequently it is reasonable to filter out the high frequency noise and remove the offsets which results in the record depicted in Figure 4(b). The three gage 6 responses during the west to east travel of all three wheel configurations are circled in Fig. 4(b) and generate Figure 4(c) for analysis.

The results in Figure 4 were obtained in test 3 shown in Figure 3. One wheel was tangential to the longitudinal joint and the other was on the opposite slab. Figure 4(c) indicates that the six-wheel gear led to the maximum top-down surface strain. In other words, the gear load, rather than the wheel load, dominates the critical top-down stress at the transverse joint.

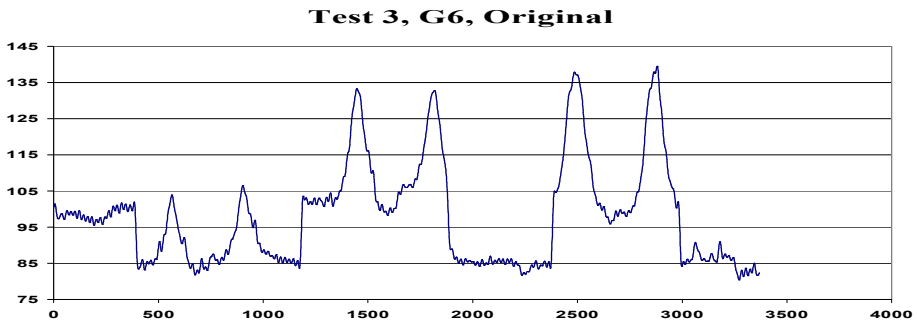

(a) Original Record.

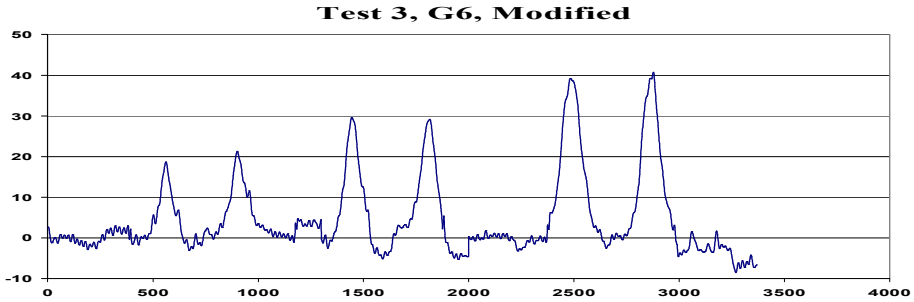

(b) Filtered and Shifted Based on Three Reference Lines in (a).

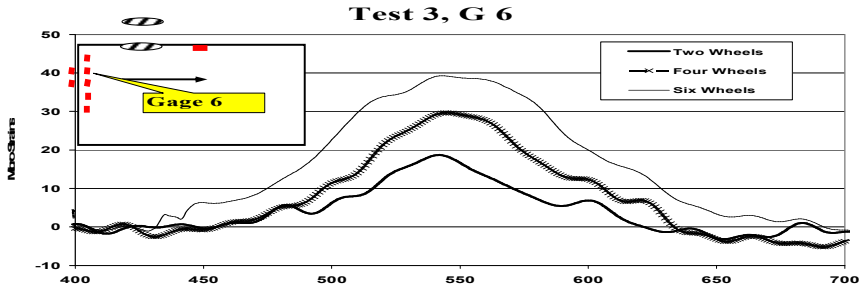

(c) Relocated the Three Marked Areas in (b) for Analysis.

Figure 4. Comparison of Strains Under Two-, Four- and Six-Wheel Gear Loads.

The strain histories of gages 3 and 6 during Test No. 6 are presented in Figure 5. Both gages were exactly under a wheel as shown in Figures 3 and 2. Since these gages can only be applied on a surface. All recorded maximum strains were in compression. Assuming the magnitude of the maximum tensile bottom strain is equal to the maximum compressive surface strain, we find that the damage potential of the three gears leading to bottom-up strains at the transverse joint was in order of: six-wheel gear greater than the four-wheel gear and the four-wheel gear greater than the two-wheel gear. The two strain histories shown in Figure 1 indicate the opposite finding at a longitudinal joint: the maximum surface strain under a two-wheel gear was higher than that under a four- and/or a six-wheel gear.

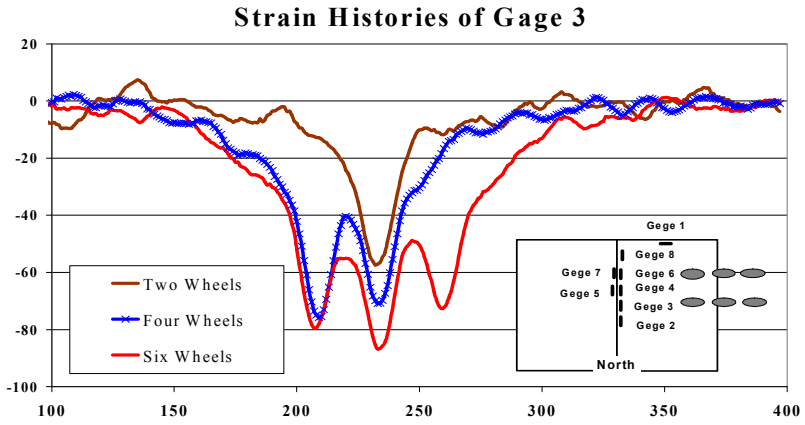

(a) Strains at Gage 3.

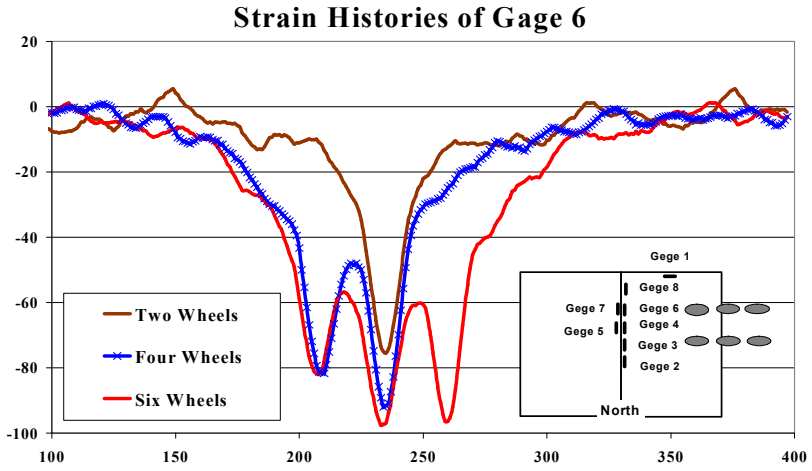

(b) Strains at Gage 6.

Figure 5. Damage Potential of Gear Configurations at Transverse Joint.

RESULTS OF TEST CONDUCTED IN MARCH, 2005

Although meaningful results were obtained in the test conducted in January, 2005, excessive noise and large aberrations in the data reduced the quality and possibly increased the introduction of errors in the final results. Consequently a more complete test plan was made utilizing two un-cracked slabs in a transition area on the south side of the test pavement. Not only slow rolling loads, but also static loads were planned. The slow rolling load locations are presented in Figure 6 (a). The first letter D indicates that the tests were under a slow rolling load. It is followed by a number from 1 to 4 which indicates load locations in the transverse direction. The last letter a, b or c indicates the wheel number two, four or six. The static load locations are presented in Figure 6 (b). The letter S indicates that the load type was two, four or six wheels, and letters SS

indicates the single wheel load. Due to the limitation of space, only results in slow rolling tests D2 (a, b and c), and in static tests SS2, S2-a (two wheels), S2-b (four wheels) and S2-c (six wheels) are presented and discussed in this paper.

The test vehicle at the FAA's NAPTF has an on board data acquisition system that records all the vehicle parameters including load magnitude, location and speed. One example of the recorded history of gear location and wheel load magnitudes from the test D-2c is presented in Figure 7. The recorded curve (a) shows the gear was moved from station 145 ft to 224 ft then back to station 145

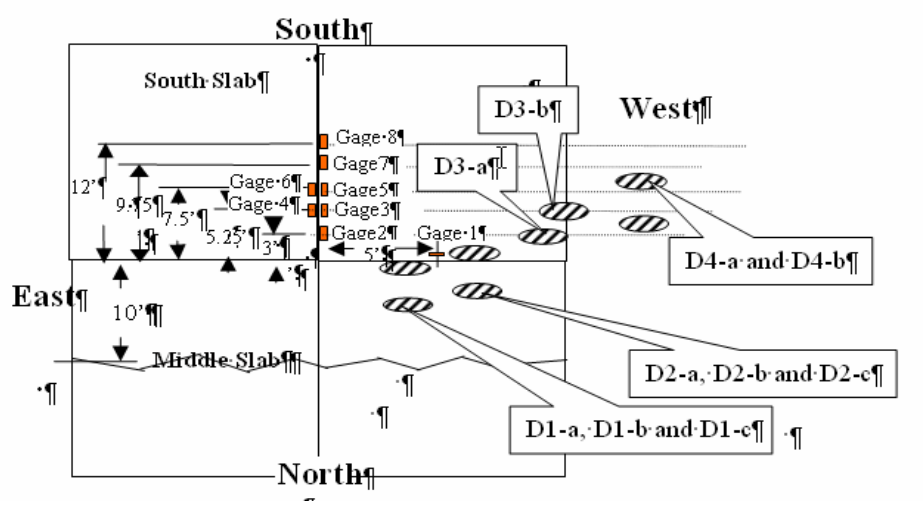

(a) Slow rolling load

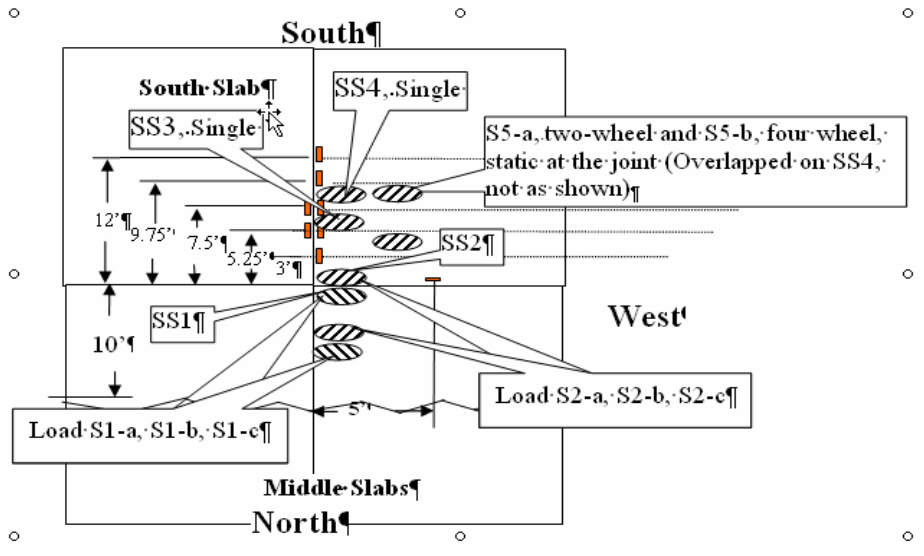

(b) Static Loads

Figure 6. Locations of Slow Rolling and Static Loads.

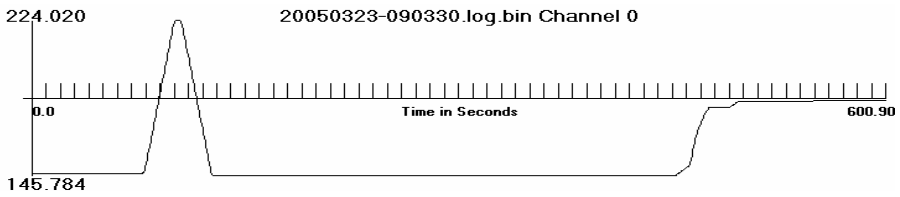

(a) Gear Location.

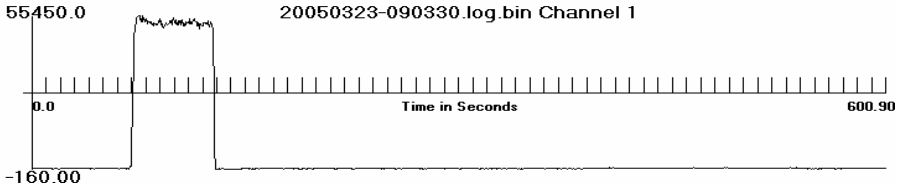

(b) Load Magnitudes of the Front Two Wheels.

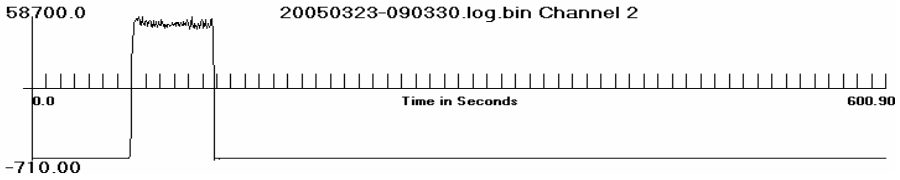

(c) Load Magnitudes of the Middle Two Wheels.

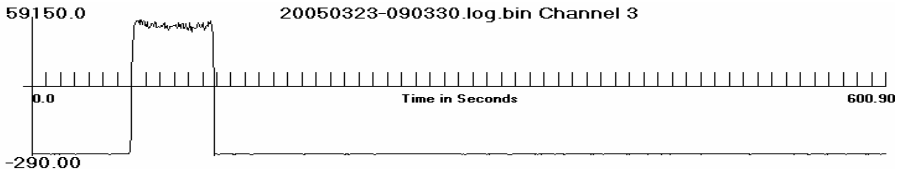

(d) Load Magnitudes of the Rear Two Wheels

Figure 7. Slow Rolling Load Histories Recorded in Test D2-c. (Six wheels were loaded.)

ft in the longitudinal direction, the total distance moved was about 79 ft. The curves in (b), (c) and (d) show the recorded wheel load magnitude histories of the front, middle and rear wheels. The figures indicate that the variation of the wheel load magnitude existed, however, the average of the magnitudes of each wheel load was close to the target value: of 55,000 lbs.

Figure 8 presents the recorded history of vehicle location and wheel loads in static test S2-c. All records started at 28 seconds after 8:43, March 23, 2005. Figure 8 (a) indicates that the vehicle was stationary during the static test. Figure 8 (b) (c) and (d) indicate that the six wheels were loaded to the target magnitude of 27,500 lbs, then after approximately 10 seconds were increased to 55,000 lbs for another 10 seconds, after which the load was removed from the pavement.

The recorded data in Figure 8 also indicates that two loadings were applied during this data acquisition. The first load application employed six wheels and the second only used two front wheels. Figure 7 and 8 are examples of the corresponding vehicle load information files that are available for every strain gage response. It should be noted that clear analysis of each gage response

requires the detailed loading information contained in the vehicle logs. These logs are all available in the FAA database [1].

Figure 9 (a) presents strain histories recorded by gage 1 at the longitudinal joint. The quality of this data was very good. With minimal noise and aberrations the plot was generated with the raw data acquired. The comparison of the three peak compressive strains at gage 1 indicates that the two-wheel gear was most critical in developing bottom-up cracks provided the maximum surface and bottom strains are assumed to be the same. The comparison of three peak tensile strains at the surface indicates that the six-wheel gear was the most critical in developing top-down cracks at the longitudinal joint.

Figure 9(b) presents the strain histories recorded by gage 3 at the transverse joint under the same slow rolling loads. Comparison of the three curves shows that the six wheel gear was the most critical in developing top-down cracks at the transverse joint. Recalling the results shown in Figure 5, we may conclude that a six-wheel gear will always be more critical, for developing both bottom-up and top-down cracks at a transverse joint than four and two-wheel gears.

(a) Gear Location.

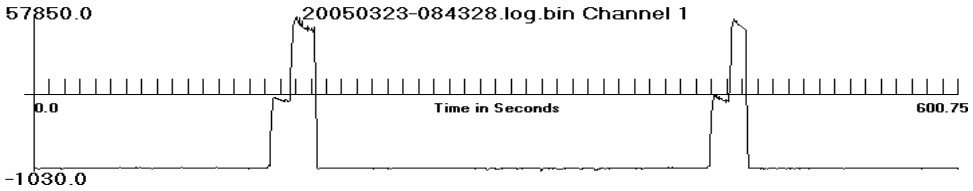

(b) Load Magnitudes of the Front Two Wheels.

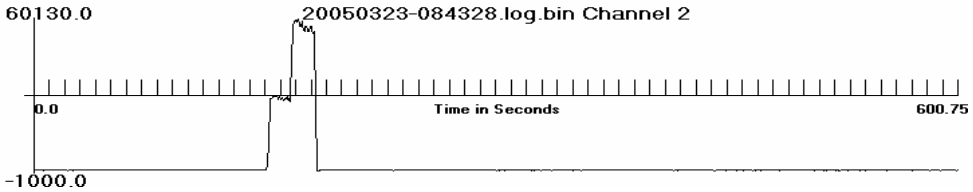

(c) Load Magnitudes of the Middle Two Wheels.

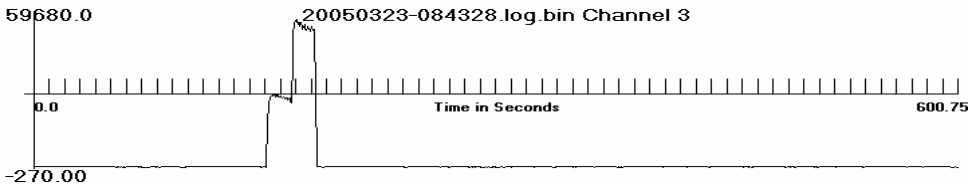

(d) Load Magnitudes of the Rear Two Wheels.

Figure 8. Static Load Histories. (Six wheels were loaded; then two wheels were loaded.)

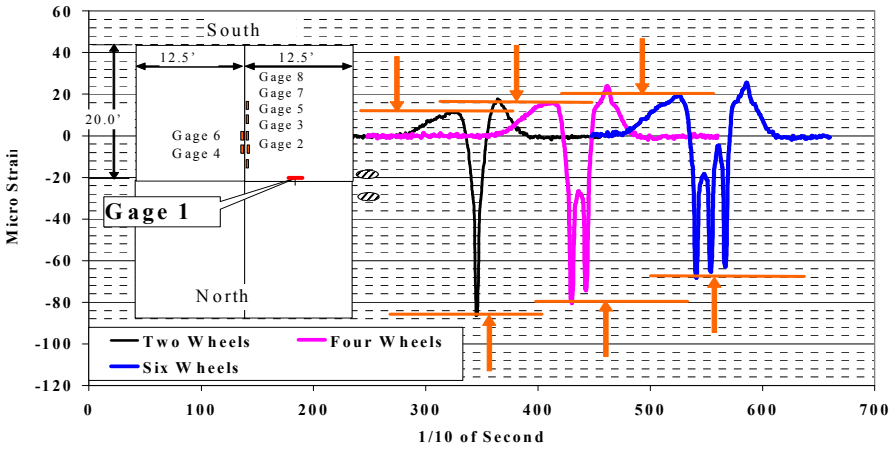

(a) Strain Histories Recorded by Gage 1.

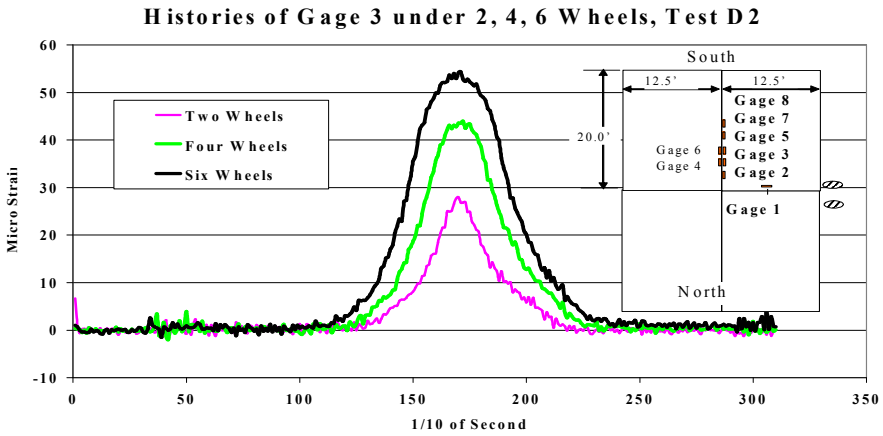

(b) Strain Histories Recorded by Gage 3.

Figure 9. Different Critical Loads at Longitudinal and Transverse Joints, Test D2.

COMPARISON BETWEEN STRAINS OBSERVED IN FULL SCALE TESTS AND 2D FINITE MODEL

After describing the surface gage applications in full scale tests conducted at the FAA's NAPTF, comparisons of the strains received in static and slow rolling tests were made with the results predicted by 2D finite element model [7] .

A device known as a "Portable Seismic Properties Analyzer" (PSPA) was used in determining the Elastic Modulus of the pavement concrete. This equipment is based on spectral analysis of surface waves method [8].

Figure 10 shows strain histories of eight surface gages (1 to 8) under the four-wheel static loads in test S2-b. The loads were applied in two steps: from zero to 27,500 lbs, and 27,500 lbs to 55,000 lbs, so the strain responses also appeared in two steps. Only surface gage 1 indicates compressive strains, while the others all indicate tensile strains. Each loading increment was applied for approximately 10 seconds. The average value of two seconds of strain data is defined as the static strain response under that load and used for comparison with the response calculated by 2D finite model.

Figure 11(a) shows the measured and calculated strain comparison under a single wheel load - test SS2 in Figure 6(b). The results at gages 3, 5, 7 and 8 (5, 7.5, 10 and 12.5 ft from the corner) are very comparable to the prediction. However, the measured strain at gage 2 (2.5 ft from the corner) is only about 50% of the prediction. Figure 11(b), (c) and (d) show similar results. The maximum strain recorded in slow rolling test D2 are also included in Figure 11(b), (c) and (d). The differences between the measured static and slow rolling maximum strain increased along with the number of wheels applied. For example, the measured maximum strain in test D2-c was higher than the static strain in test S2-c. The difference suggests that the selected static load location was not the critical location of the corresponding slow rolling load. For the two-wheel cases, the selected static load was located closest to the critical location of the slow moving load, so their maximum strains are closest. However, for the six-wheel case, the critical load location of the slow rolling test might be a significant distance away from the selected static load. Therefore, the measured strains under a slow rolling load should be compared with the predicted ones under the same slow rolling load.

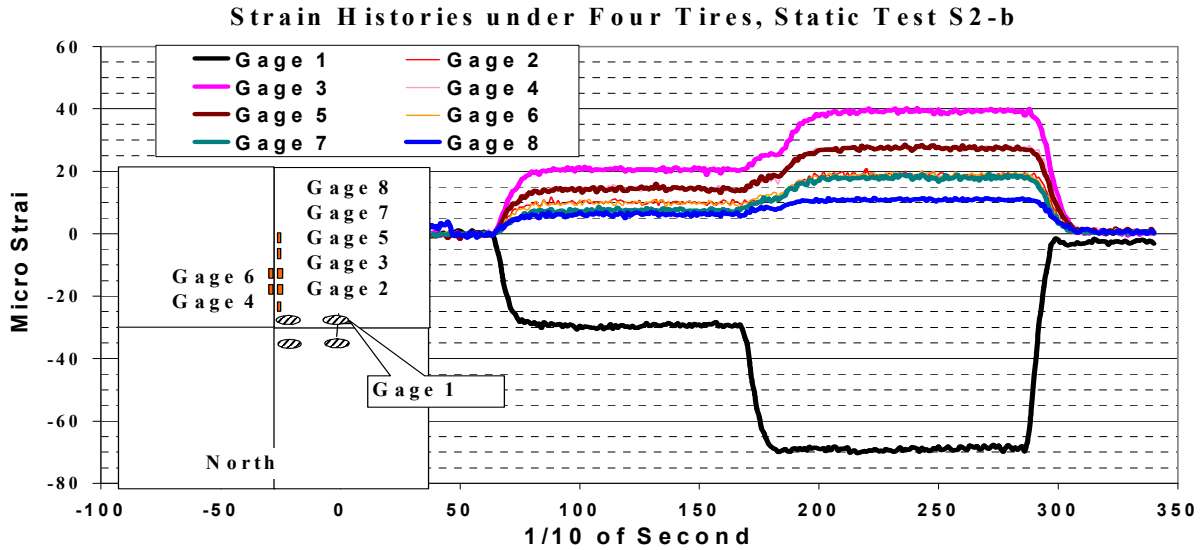

Figure 10. Eight Strain Histories Under Static Test S1-b, Four Wheels.

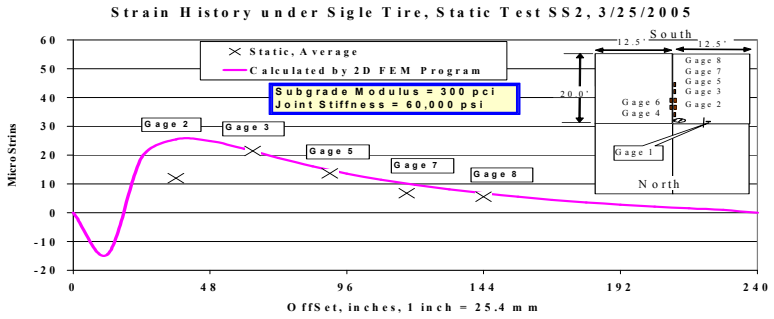

(a) Under a Single Wheel.

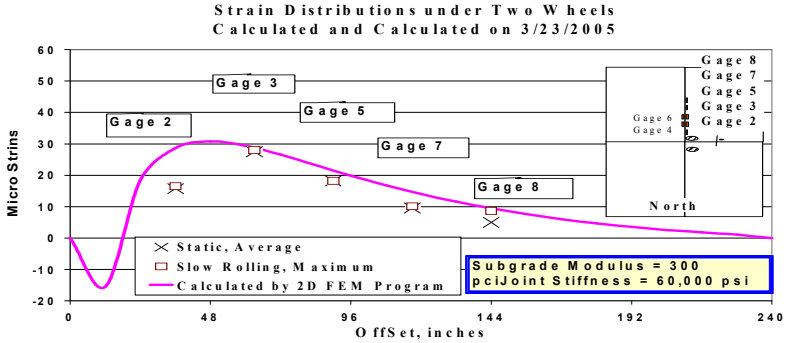

(b) Under Two Wheels.

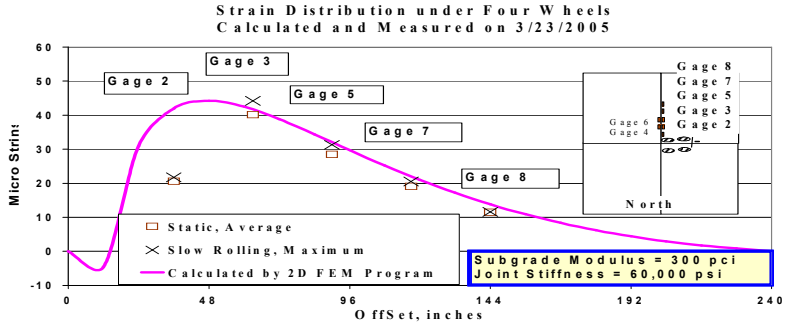

(c) Under Four Wheels.

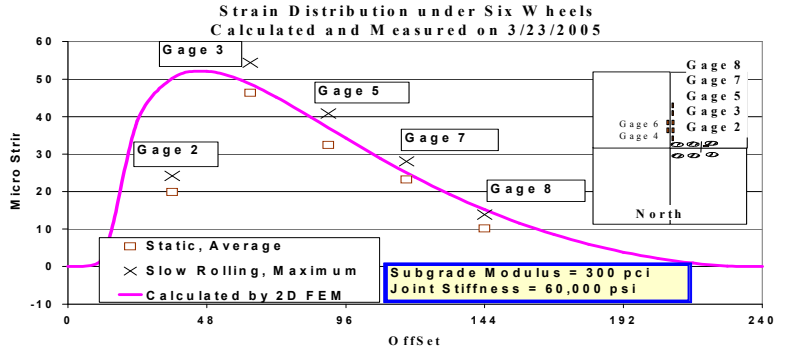

(d) Under Six Wheels.

Figure 11. Comparison of the Measured and Calculated Strain Distributions Under Static Loads.

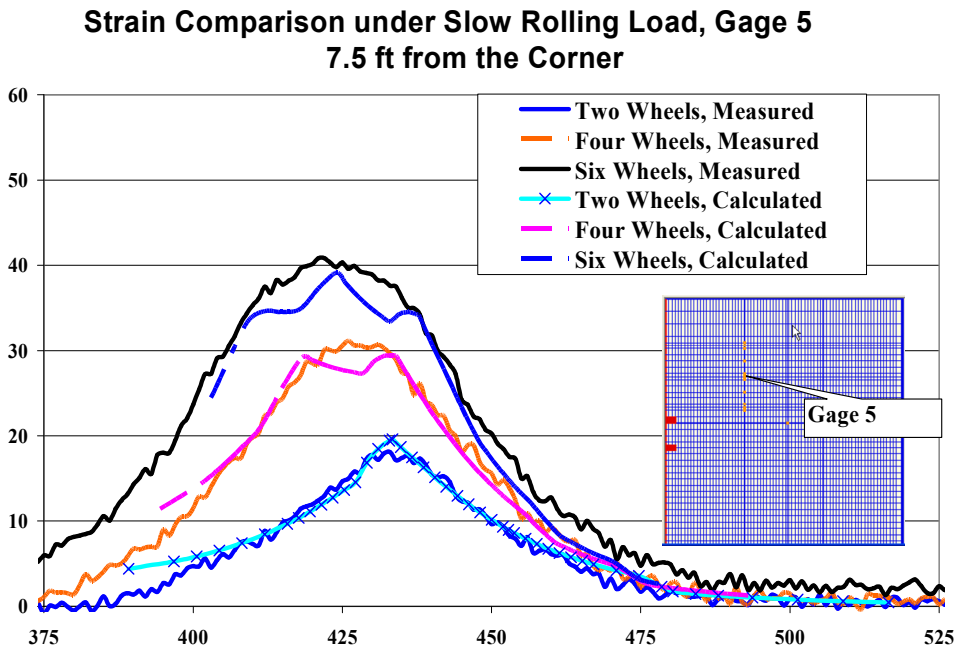

(a) Gage 5, 7.5 feet from the Corner.

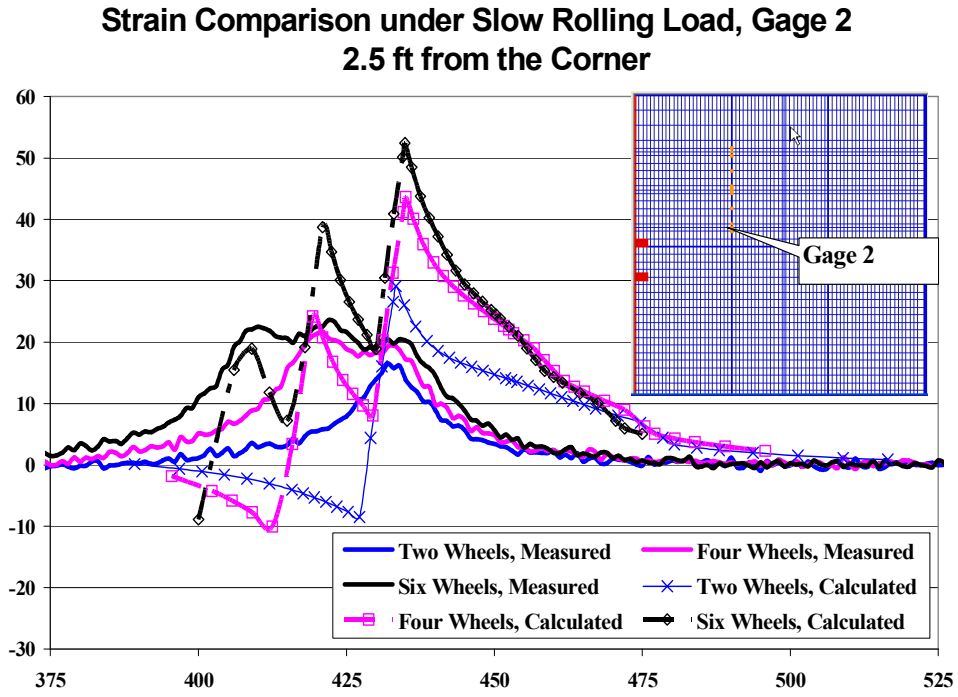

(b) Gage 2, 2.5 feet from the Corner.

Figure 12. Comparison of Measured and Calculated Strain Time Histories.

The measured and predicted strain responses at gage 5 (7.5 ft from the corner) and gage 2 (2.5 ft from the corner) under a slow rolling load (test D2 in Figure 6(a)) are presented in Figure 12. Figure 12 (a) indicates that the measured and predicted slow rolling strains at gage 5 match well. However, the predicted results were more sensitive to the number of axles. The predicted strain curves under four and six wheels show two and three peaks while the measured results show only "one peak" for all three loads. The predicted strains were more sensitive to the gear axles for strains at gage 2 in Figure 12 (b). The inverse bending behavior can be clearly observed in all three calculated curves: The strain histories at gage 2 start from zero, go negative then cross over the X axis then reach the positive peak values.

Why do the significant differences exist? They may be caused by the difference between the assumptions used in the 2D model and the real pavement. Three aspects are worth considering: thin plate model used for the pavement surface layer, dense liquid model for the pavement foundation and/or the shear or dowel model for the pavement joint. How critical each factor is needs further study.

CONCLUSIONS

Surface strain gages can provide direct strain measurement on a slab surface. Their reliability is comparable to the full bridge embedded type gages, when used dynamically, in other words when temperature compensation is not an issue. The cost of the quarter bridge surface mounted gages is a fraction of the embedded type. After experiences accumulated in two tests, all eight surface strain gages in the third test showed outstanding performance. The surface gages always performed well when a wheel was moving near by but not directly on the gages. All gages also performed well when a wheel was rolled over it once or twice. If a surface gage was installed appropriately and with proper protection for the gage surface, satisfactory performance after ten wheel load passes was achieved. This is enough to obtain information on pavement critical responses.

Two major findings can be summarized in application of the surface strain gages. First, the surface gage results verify that aircraft gear load damage potentials are different at the transverse and longitudinal joints. At a transverse joint, both top-down and bottom-up cracks are dominated by the gear load. At a longitudinal joint, the top-down cracks are still dominated by the gear load while the bottom-up cracks are dominated by the wheel load. Second, though 2D finite element can simulate well the pavement strain responses under both static and slow rolling loads, significant differences have been observed in predicting top-down surface strain at a transverse joint near a corner. The pavement behavior that leads to the significant difference needs further study.

ACKNOWLEDGEMENTS

The FAA Airport Technology R&D Branch Manager, Dr. Satish K. Agrawal, supported the work described in this paper. The contents of the paper reflect the views of the authors, who are responsible for the facts and accuracy of the data presented within. The contents do not necessarily reflect the official views and policies of the FAA. This paper does not constitute a standard, specification, or regulation. Special thanks are also given to Dr. Gordon Hayhoe for his technical leadership in planning the tests, to Dr. David Brill for his valuable comments after

reviewing the paper, to Mr. Chuck Teubert for his leadership in managing the construction and testing. Our sincere thanks are also given to all those who have provided valuable assistance during the construction and testing but not mentioned above.

REFERENCES

1. http://www.airporttech.tc.faa.gov/naptf/
2. Fabre, M.C,. Maurice, M.J,.Guedon, M.D,.Mazars M.A and.Petitjean M.J. "A380 Pavement Experimental Programme, Rigid Phase," Technical Report, Jan. 2005
3. Grasley, Zachary. Internal Relative Humidity, Drying Stress Gradients, and Hygrothermal Dilitation of Concrete, Masters Thesis, University of Illinois at Urbana-Champaign, 2003.
4. USACOE. "Lockbourne No.1 Test Track, Final Report," US Army Engineer, Ohio River Division Laboratories, Mariemont, Ohio. 1946
5. Guo, E. H. and F. Pecht, "Critical Gear Configurations and Locations for Rigid Airport Pavements - Observations and Analyses," GeoShanghai International Conference, ASCE Specialty Proceeding: Pavement Mechanics and Testing, June 6-8, Shanghai, China 2006.
6. Timoshenko, Stephen P., "History of Strength of Materials," Dover Publications, Inc., New York. 1953
7. Guo, Edward H & May Dong, "JSLAB-2002 Technical Report", under contract DTFH61-01-P-00255 with the Federal Highway Administration, 2002
8. Nazarian, S., Yuan, D., Baker, M. R., "Rapid Determination of Pavement Moduli with Spectral-Analysis-of-Surface-Waves Method", Report Research Project 0-1243, the Center of Geotechnical and Highway Materials Research, The University of Taxes at El Paso, El Paso, TX, November, 1995.
9. Westergaard, H.M, "Stress in Concrete Pavements Computed by Theoretical Analysis", Annual Meeting of the Highway Research Board, National Research Council, Washington D.C., Dec., 1925